IEEE Photonics Journal
An IEEE Photonics Society Publication

Open Access

Coupled-Mode Analysis of the Low-Loss Plasmon-Triggered Switching Between the 0^{th} and -1^{st} Orders of a Metal Grating

Volume 7, Number 4, August 2015

Alexandre V. Tishchenko
Olivier Parriaux

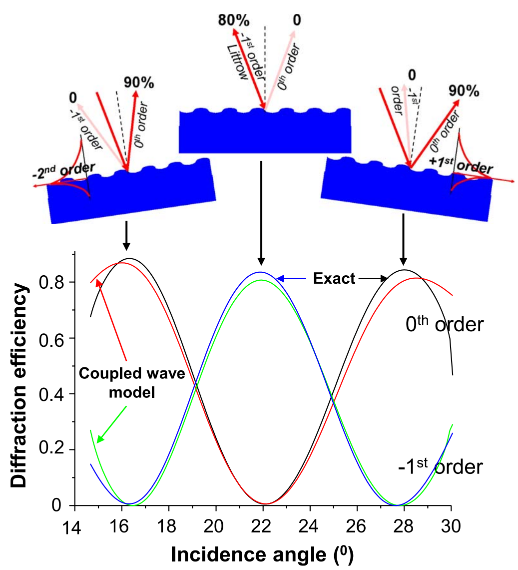

DOI: 10.1109/JPHOT.2015.2445766
1943-0655 © 2015 IEEE

Coupled-Mode Analysis of the Low-Loss Plasmon-Triggered Switching Between the 0^{th} and -1^{st} Orders of a Metal Grating

Alexandre V. Tishchenko and Olivier Parriaux

Laboratoire Hubert Curien, UMR Centre National de la Recherche Scientifique 5516, Université de Lyon, 42000 Saint-Étienne, France

DOI: 10.1109/JPHOT.2015.2445766

Manuscript received April 29, 2015; revised June 5, 2015; accepted June 10, 2015. Date of publication June 16, 2015; date of current version July 2, 2015. Corresponding author: A. Tishchenko (e-mail: tishchen@univ-st-etienne.fr).

Abstract: A coupled-wave analysis of the particularly low-loss 0^{th}- and -1^{st}-order switching triggered by the $+1^{st}$- and -2^{nd}-order excitation of the surface plasmon of an undulated metal surface reveals that the cancelation of the -1^{st}-order diffraction efficiency is due to the destructive interference between the field directly diffracted by the grating and the field coupled to a plasmonic supermode then radiated away by the grating in the direction of the -1^{st} order, the plasmon outcoupling length being much shorter than the absorption length of the excited plasmonic supermode.

Index Terms: Gratings, plasmonics, switching.

1. Introduction

A new plasmonic effect involving a non-localized plasmon excited by a deep sinusoidal metal grating was found numerically and confirmed experimentally [1]: When excited by the -2^{nd} or the $+1^{st}$ grating order, the plasmon triggers a high contrast switching between the reflected free-space 0^{th} and -1^{st} orders upon a tilt of the incidence angle or a wavelength scan. The remarkable characteristic of this high-contrast plasmon coupling effect is to be quasi-lossless, while plasmon coupling by a grating is usually associated with a strong resonant absorption. To gain a physical understanding of the underlying coupling and switching mechanism, a coupled-wave analysis was developed. The analysis and the phenomenological interpretation it permits to derive are presented in the present paper.

2. Description of the Plasmon-Triggered Effect

The switching effect occurs on either side of the -1^{st} order Littrow condition, assuming a fixed wavelength λ and a variable incidence angle θ in an incidence medium of refractive index 1. The Littrow angle $\theta = \theta_L$ is given by

$$\sin\theta_L = \lambda/2\Lambda \tag{1}$$

where Λ is the sinusoidal grating period.

It is known that at the Littrow angle the diffraction efficiency of the -1^{st} order of a sinusoidal metal grating increases with the grating depth d up to a maximum corresponding to a

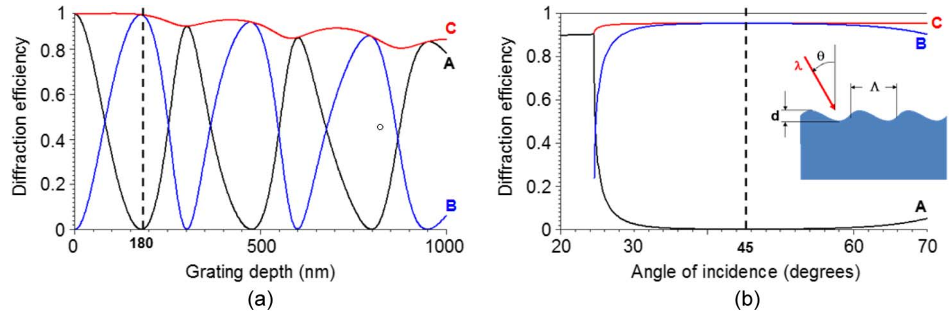

Fig. 1. TM 0^{th} and -1^{st}-order diffraction efficiency (curves A and B, respectively) of a sinusoidal silver grating of 447 nm period at 633 nm wavelength sketched in the insert; curve C illustrates the total propagating power (i.e., 1 minus the absorption losses). (a) Depth dependence in the auto-collimation mount $\theta_L = 45°$. (b) Angular spectra around the Littrow angle θ_L at the grating depth $d_m = 180$ nm.

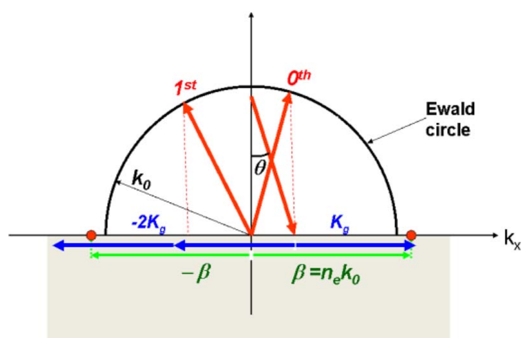

Fig. 2. Ewald circle in the reciprocal space with propagating 0^{th} and -1^{st} orders and the condition $3K_g > 2\beta$. The red spots locate the forward and backward propagating plasmons of propagation constant β.

cancelation of the 0^{th} order Fresnel reflection [2]. Then, the diffraction efficiency oscillates periodically between zero and maxima provided there are no other propagating diffraction orders. Such depth dependence occurs for both TM and TE polarizations (note that the first maximum of the -1^{st} order occurs at a grating depth d_m which is notably smaller for the TM than for the TE polarization). Fig. 1(a) shows the depth dependence of the 0^{th} and -1^{st} orders of a sinusoidal silver grating of period $\Lambda = 447$ nm on which a TM plane wave of 633 nm wavelength impinges under the angle θ_L of 45 degrees. The grating depth of first maximum -1^{st} order efficiency d_m is 180 nm (it is 750 nm for the TE polarization).

Setting the grating at the depth d_m of the first maximum of the -1^{st} order efficiency and scanning the incidence angle around θ_L gives as expected a quite large and smooth angular width of the also called auto-collimation mount as shown in Fig. 1(b) with the -1^{st} order cutoff at $\sin\theta = 2\sin\theta_L - 1$ (here $\theta = 24.5°$).

The 0^{th} and -1^{st} order angular spectra change dramatically if the Littrow angle is smaller than in the above example and if three times the grating K-vector $K_g = 2\pi/\Lambda$ is only slightly larger than twice the plasmon propagation constant $\beta = n_e k_0$ where $k_0 = 2\pi/\lambda$ and n_e is the effective index of the plasmon with n_e slightly superior to 1 in the present case of an air incidence medium:

$$3K_g > 2\beta. \tag{2}$$

This condition is illustrated in the Ewald circle of Fig. 2, where it can be seen that the 0^{th} and -1^{st} orders are always propagating and that the plasmon can either be coupled codirectionally by the $+1^{st}$ order or contradirectionally by the -2^{nd} order.

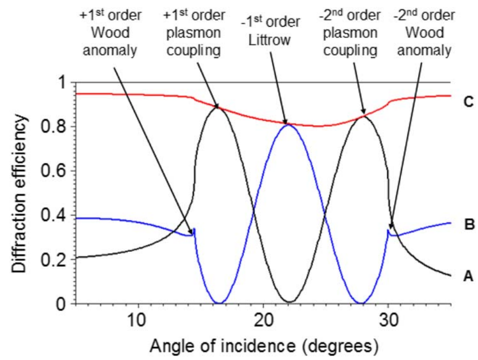

Fig. 3. Angular spectra of the reflected 0th (curve A) and -1st orders (curve B) of a sinusoidal silver grating with the situation prevailing in the reciprocal space for each specific feature. The considered complex permittivity ε_m of silver at $\lambda = 633$ nm wavelength is $\varepsilon_m = -16.1 + i\ 1.1$. $\Lambda = 844$ nm, and $d = 240$ nm.

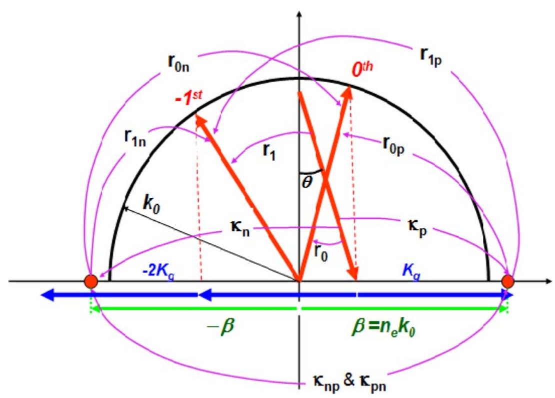

Fig. 4. Definition of reflection coefficients, the propagation constants and the coupling coefficients between incident, reflected, and plasmon waves.

As shown in a synthetic figure [1, Fig. 4] and repeated here in a simplified form as Fig. 3 for sake of clarity, the exact modeling of the angular spectrum of a sinusoidal silver grating in the neighborhood of the -1st order Littrow mount reveals striking differences with respect to the above spectra of Fig. 1(b) which was not explained in [1].

Whereas the -1st order (curve B) still has its maximum at the Littrow angle of 24 degrees, its efficiency drops sharply to zero under the conditions of +1st and -2nd order plasmon coupling of the incident wave where the 0th reflected order (curve A) reaches a maximum. This is in sharp contrast with Fig. 1(b) where the -1st order efficiency remains large over a wide angular domain. More striking even is exhibited by the "balance" curve C (the balance corresponds to 1 minus the absorption): uncommonly, the largest absorption loss does not occur at the synchronous excitation of the lossy plasmon, but in-between, where the plasmon is not excited. In order to gain a phenomenological understanding of the coupling mechanism at the origin of these unexpected characteristics, a coupled mode model has been developed.

3. Coupled Mode Representation

The waves considered in the coupled wave model in the angular range between the two Wood anomalies are the incident plane wave, the 0th order Fresnel reflected wave, the forward- and the backward-propagating plasmon modes of propagation constant β. These are represented by their wave vectors in the reciprocal space in Fig. 4 together with the coupling coefficients κ_{ij}

between them. The radius of the Ewald circle is k_0 since the outer medium is assumed to be vacuum or air.

As the arrows indicate, κ_p, κ_n stand for the $+1^{st}$ and -2^{nd} order in-coupling coefficients between the incident wave and the forward, resp. backward plasmons.

The plasmon field amplitudes in the propagation directions $+$ and $-$ x are defined as

$$\begin{aligned} a_p(x) &= a_{0p}(x)\exp(i\beta x) \\ a_n(x) &= a_{0n}(x)\exp(-i\beta x). \end{aligned} \tag{3}$$

The rate of variation of the plasmon field amplitudes is

$$\begin{cases} \frac{da_{0p}}{dx} = \kappa_p f(x)\exp[i(k_0\sin\theta + K - \beta)x] - \alpha a_{0p}(x) + \kappa_{pn} a_{0n}(x)\exp[i(3K - 2\beta)x] \\ \frac{da_{0n}}{dx} = -\kappa_n f(x)\exp[i(k_0\sin\theta - 2K + \beta)x] + \alpha a_{0n}(x) + \kappa_{np} a_{0p}(x)\exp[i(2\beta - 3K)x] \end{cases} \tag{4}$$

where $f(x)$ is the field amplitude profile of the incident wave on the axis x, α the real absorption loss coefficient of the plasmon mode, and the coefficients κ_{np} and κ_{pn} stand for the inter-plasmon coupling by the 3^{rd} diffraction order. The grating vector K_g is simply written K in what follows. As the retrieval of the phenomenological parameters represented in Fig. 4 from the exact spectra of Fig. 3 will not require a normalization of the fields, the field amplitudes as well as f(x) are considered here to be dimensionless. The coupling coefficients and the spatial frequencies are expressed in μm^{-1} as retrieved in Section 4.

The resulting amplitudes $A_0(x)$ and $A_1(x)$ of the 0^{th} and -1^{st} orders write as follows after using the r_{ij} coefficients defined in Fig. 4:

$$\begin{aligned} A_0(x) &= r_0 f(x) + r_{0p}(x)a_{0p}(x)\exp[i(\beta - K - k_0\sin\theta)x] + r_{0n}(x)a_{0n}(x)\exp[i(-\beta + 2K - k_0\sin\theta)x] \\ A_1(x) &= r_1 f(x) + r_{1p}(x)a_{0p}(x)\exp[i(\beta - K - k_0\sin\theta)x] + r_{1n}(x)a_{0n}(x)\exp[i(-\beta + 2K - k_0\sin\theta)x]. \end{aligned} \tag{5}$$

Making the change of field amplitudes a_{0p} and a_{0n} to the new field amplitudes $\tilde{a}_p$ and $\tilde{a}_n$

$$\begin{aligned} a_{0p}(x) &= \tilde{a}_p(x)\exp[i(k_0\sin\theta + K - \beta)x] \\ a_{0n}(x) &= \tilde{a}_n(x)\exp[i(k_0\sin\theta - 2K + \beta)x] \end{aligned} \tag{6}$$

permits lightening differential equations (4)

$$\begin{cases} \frac{d\tilde{a}_p}{dx} = \kappa_p f(x) + i(k_p - k - K)\tilde{a}_p(x) + \kappa_{pn}\tilde{a}_n(x) \\ \frac{d\tilde{a}_n}{dx} = -\kappa_n f(x) - i(k_p + k - 2K)\tilde{a}_n(x) + \kappa_{np}\tilde{a}_p(x) \end{cases} \tag{7}$$

where $k_p = i\alpha + \beta$ stands for the complex propagation constant of the plasmon mode and $k = k_0\sin\theta$ for the x-projection of the incident wave k-vector and to express the 0^{th} and -1^{st} order amplitudes as

$$\begin{aligned} A_0(x) &= r_0 f(x) + r_{0p}(x)\tilde{a}_p(x) + r_{0n}(x)\tilde{a}_n(x) \\ A_1(x) &= r_1 f(x) + r_{1p}(x)\tilde{a}_p(x) + r_{1n}(x)\tilde{a}_n(x). \end{aligned} \tag{8}$$

Equation (7) can be decoupled by defining two supermode field amplitudes $\tilde{a}_\pm$

$$\tilde{a}_\pm = \tilde{a}_p + \gamma_\pm \tilde{a}_n \tag{9}$$

where

$$\gamma_\pm = (i\Delta \pm D)/\kappa_{np} \tag{10}$$

$$\Delta = (3K - 2k_p)/2 \tag{11}$$

$$D = \sqrt{\kappa_{pn}\kappa_{np} - \Delta^2}. \tag{12}$$

Then, defining

$$\kappa_\pm = \kappa_p - \gamma_\pm \kappa_n \tag{13}$$

the separated equations governing the rate of variation of the supermode amplitudes $\widetilde{a}_\pm$ become:

$$\frac{d\widetilde{a}_\pm}{dx} = \kappa_\pm f(x) + \left[-i\left(k - \frac{K}{2}\right) \pm D\right]\widetilde{a}_\pm. \tag{14}$$

Assuming plane wave incidence, $f(x) = 1$, the solutions of (14) are

$$\widetilde{a}_\pm = \frac{-i\kappa_\pm}{k - \frac{K}{2} \pm iD} = \frac{-i\kappa_\pm}{k - k_\pm} \tag{15}$$

where

$$k_\pm = \frac{K}{2} \mp iD. \tag{16}$$

Expression (15) has a polar form where $k_\pm$ are the pole coordinates of the supermode amplitudes.

Having solved (14) for the supermode amplitudes $\widetilde{a}_\pm$, the individual plasmon amplitudes $\widetilde{a}_p$ and $\widetilde{a}_n$ defined in (6) can now be retrieved separately using expressions (10) to (12) for γ, and in the polar form of (15), which will ease the bridging between the coupled wave formalism established above and the exact solution which led to the angular spectrum represented in Fig. 3

$$\begin{aligned} \widetilde{a}_p &= \frac{(-i\Delta + D)\widetilde{a}_+ + (i\Delta + D)\widetilde{a}_-}{2D} = \frac{v_p^+}{k - k_+} + \frac{v_p^-}{k - k_-} \\ \widetilde{a}_n &= \frac{\kappa_{np}(\widetilde{a}_+ - \widetilde{a}_-)}{2D} = \frac{v_n^+}{k - k_+} + \frac{v_n^-}{k - k_-} \end{aligned} \tag{17}$$

where

$$v_p^\pm = -\kappa_\pm \frac{\pm\Delta + iD}{2D} \tag{18}$$

$$v_n^\pm = \mp \frac{i\kappa_\pm \kappa_{np}}{2D} \tag{19}$$

are the pole magnitudes of the individual plasmon modes expressed in μm^{-1}.

4. Retrieval of the Coupling Coefficients

Expressions (15) for the separate plasmon field amplitudes $\widetilde{a}_p$ and $\widetilde{a}_n$ contain the poles of the two supermodes defined above. The bridging procedure between exact electromagnetic and coupled wave solutions is now to extract the singular part of the exact solution from its regular part, to match the former with the polar expressions (17), and to determine all coupling κ_{ij} and reflection r_{ij} coefficients. An important point will be to check whether the retrieved κ_{ij} and r_{ij} are relevant phenomenological parameters in the coupled wave model in that they remain reasonably constant over a large enough domain of variation of the optogeometrical parameters of the structure. Such behavior of the phenomenological parameters is not a priori predictable since the grating here is not just a small perturbation of a flat metal surface. Once the coupled wave model has been checked to be relevant, it will provide a meaningful interpretation of the coupling mechanism and of its features.

Before undertaking the actual determination of the phenomenological parameters, we will derive a few useful relationships between them.

From (16), one gets the expressions of D and K in terms of the supermode pole coordinates $k_{\pm}$:

$$D = -\frac{k_+ - k_-}{2i}, \quad K = k_+ + k_-. \tag{20}$$

Dividing equalities in (18), one obtains the expressions of ratios κ_-/κ_+ and $(\Delta - iD)/(\Delta + iD)$ in terms of the pole magnitudes of the individual plasmon modes:

$$\begin{aligned} \kappa_-/\kappa_+ &= -\frac{v_n^-}{v_n^+} \\ \frac{(\Delta - iD)}{(\Delta + iD)} &= \frac{v_p^- v_n^+}{v_p^+ v_n^-}. \end{aligned} \tag{21}$$

Then, from (20) and the second expression of (21), parameter Δ can be expressed in terms of the supermode pole coordinates and the individual mode amplitudes:

$$\Delta = iD\frac{\left(v_p^+ v_n^- + v_p^- v_n^+\right)}{\left(v_p^+ v_n^- - v_p^- v_n^+\right)} = -\frac{k_+ - k_-}{2}\frac{\left(v_p^+ v_n^- + v_p^- v_n^+\right)}{\left(v_p^+ v_n^- - v_p^- v_n^+\right)}. \tag{22}$$

This permits the expression of the complex propagation constant k_p of the individual plasmon using the definition of Δ in (11):

$$k_p = \frac{3}{2}K - \Delta, \quad \text{i.e.,}\ \alpha = -\mathrm{Im}(\Delta)\ \text{and}\ \beta = \frac{3}{2}K - \mathrm{Re}(\Delta). \tag{23}$$

Rewriting (18) and using (22), $\kappa_{\pm}$ can now be fully expressed in terms of the pole amplitudes of the individual plasmon modes:

$$\kappa_{\pm} = i\left(v_p^{\pm} - v_p^{\mp}\frac{v_n^{\pm}}{v_n^{\mp}}\right). \tag{24}$$

From (18), (22), and (24), the inter-plasmon coupling coefficients κ_{np} and κ_{pn} can now be explicitly expressed in terms of pole coordinates and magnitudes:

$$\begin{aligned} \kappa_{np} &= \frac{2Dv_n^+}{-i\kappa_+} = \frac{2Dv_n^+ v_n^-}{\left(v_p^+ v_n^- - v_p^- v_n^+\right)} \\ \kappa_{pn} &= \frac{\Delta^2 + D^2}{\kappa_{np}} = \frac{2Dv_p^+ v_p^-}{\left(v_p^- v_n^+ - v_p^+ v_n^-\right)}. \end{aligned} \tag{25}$$

Finally, the coupling coefficients κ_p and κ_n of the incident wave to the individual plasmon modes can be expressed from the definition of $\kappa_{\pm}$ in (13) and using (25):

$$\begin{aligned} \kappa_p &= \frac{\kappa_-(i\Delta + D) - \kappa_+(i\Delta - D)}{2D} = i\left(v_p^+ + v_p^-\right) \\ \kappa_n &= \frac{\kappa_{np}}{2D}(\kappa_- - \kappa_+) = -i\left(v_n^- + v_n^+\right). \end{aligned} \tag{26}$$

The procedure of retrieval of the phenomenological coefficients consists in the following steps. A rigorous electromagnetic solution of the diffraction on a sinusoidal metallic structure under TM incidence is first obtained by means of the Rayleigh method shown to be exact well beyond the long-pretended validity limit [3]. An analysis of the exact solution performs the separation between its regular and singular parts according to the procedure described in detail in [4]. Then, the latter is used to retrieve the pole coordinates k_+ and k_+, and the pole amplitudes $v_p^{\pm}$ and $v_n^{\pm}$ from where the plasmon propagation constant k_p is obtained from (23), and

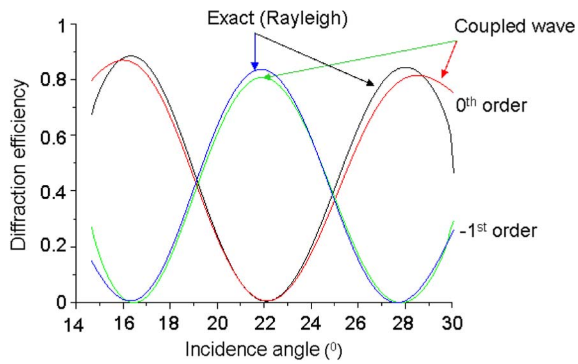

Fig. 5. Comparative angular spectra between exact and coupled-mode modeling with the same data as in Fig. 3.

the coupling coefficients κ_p, κ_n, κ_{pn}, and κ_{np} are determined using (25) and (26). Note that the numerical value of each coupling coefficient depends on the definition of the amplitudes of two coupled waves. As the objective of the present work is limited to providing a physical understanding of the remarkable features of the said plasmon-triggered switching, we have left aside the question of the normalization of the amplitudes of all waves involved in the coupling mechanism.

Introducing the phenomenological parameters into the coupled-wave equations (5) for A_0 and A_1 leads to the 0^{th} and -1^{st} angular spectra shown in Fig. 5 in comparison with the exact solution. The spectra almost coincide with a slight difference on the angle at which the -1^{st} order efficiency cancels and on the maximum amplitude of the 0^{th} and -1^{st} orders. The difference between the total diffraction efficiency and its singular part corresponds to the regular part of the meromorphic function representing the efficiency. This regular part corresponds to the non-resonant contributions to the total efficiency. Since our phenomenological analysis is based on the sole resonant response, the regular part is considered as constant in the whole angular domain.

Two criteria for the validity of a coupled-mode representation of the operation of the plasmon-mediated switch have been checked to be satisfied: the first validity criterion is satisfied in that the phenomenological parameters κ_{ij}, r_{ij}, κ_p, κ_n remain essentially constant upon a moderate variation of the wavelength and of the period; this was not a priori evident since a metal corrugation as deep as 28% of the period and 38% of the wavelength is far from a small perturbation of a flat metal surface; such ratios can still be considered as those of a weak perturbation in a dielectric grating waveguide of moderate guidance; however, in non-localized plasmon propagation, the sharp boundary conditions applied where the modal field is maximum lead to a strong modal field perturbation even at an undulation depth smaller than in the present structure The second validity criterion concerns the choice of the points where the matching is made between the rigorous and the coupled-mode solutions; it was checked that the parameters κ_{ij} and r_{ij} are essentially independent of the points as long as these cover the 15–30° angular range uniformly.

The examination of the phenomenological parameters corresponding to the spectra of Fig. 5 reveals the electromagnetic mechanism operating in the 0^{th} and -1^{st} free space order switching effect. Fig. 4 is reproduced in Fig. 6 with the quantitative values found for the parameters. The following observations can be made.

a) The modulus of the coefficients r_{0p} and r_{0n} mainly contributing from the two plasmon modes to the 0^{th} order is 0.47 and 0.51, respectively.
b) The modulus of the coefficients r_{1p} and r_{1n} mainly contributing to the -1^{st} order is 0.51 and -0.5, respectively.
c) The direct coupling coefficient r_0 and r_1 from the incident plane wave to the 0^{th} and -1^{st} orders are relatively very weak which implies from a) and b) above that the conditions are suitable for destructive interference when their phases are π phase-shifted as they are at the angles of 16 and 28 degrees for the -1^{st} order and 22 degrees for the 0^{th} order.

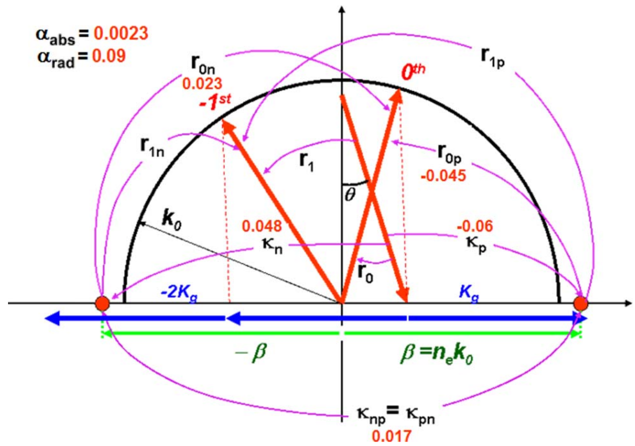

Fig. 6. Quantitative values of the phenomenological parameters corresponding to the spectra of Fig. 5 expressed in the Ewald circle. The coupling coefficients and spatial frequencies are in μm^{-1}.

d) $\kappa_{pn} = \kappa_{np} = 0.017$ μm^{-1}. This third order inter-plasmon coupling coefficient is rather large considering that the grating profile is sinusoidal. It is weaker than the coupling coefficients κ_p and κ_n of the incident wave to the co- and counter-propagating plasmons; however the inter-plasmon coupling is resonant which implies that this coupling can be strong in the present configuration where the detuning is small. This illustrates why the two individual plasmons cannot be excited separately and justifies a posteriori the resort to the super-modes of amplitudes $\tilde{a}_{\pm}$.
e) The clue about the quasi-lossless plasmonic mediation in the switching mechanism is revealed when extracting the absorption coefficient $\alpha_{abs} = 0.0023$ μm^{-1} of the plasmon and its radiation coefficient $\alpha_{rad} = 0.09$ μm^{-1}. This means that the radiation length of the plasmon is about 40 times shorter than its absorption length which implies that the field coupled to the plasmons by the +1st and -2nd orders is re-radiated into the propagating 0th and -1st orders well before it is absorbed.

5. Conclusion

The coupled-mode model of a deep sinusoidal metal grating diffracting two free-space orders in the neighborhood of the -1st order Littrow mount permits to understand phenomenologically how the switching between the 0th and -1st TM orders operates with the mediation of -2nd and +1st order plasmon excitation. It also elucidates why this plasmon-triggered switching effect exhibits quasi-zero excess loss; the reason lies in the propagating plasmon radiation strength of the grating being notably larger than the absorption rate of the plasmon thanks to the large depth of the sinusoidal grating. The switching mechanism can therefore be understood as a constructive/destructive interference in the 0th and -1st order directions between the plasmon fields quickly re-radiated into free space. The coupling mechanism revealed by this analysis enables the design of a set of devices made of various metals in different spectral ranges in application fields such as security devices, opto-mechanical actuators where the spectral width of the switch is compatible with LED sources. The coupled-mode model is developed here in the angular domain, but the use of the switching effect is naturally expandable to the wavelength domain under constant incidence angle as shown experimentally in [1] since a wavelength scan can switch the element from the -1st order Littrow mount to the condition of -2nd or +1st order plasmon excitation with the advantage of much faster operation than in the angular domain. A further and unexpected outcome of the present phenomenological analysis is the possibility of generating the switching effect for the TE polarization as well, despite the non-existence of a plasmon mode; this will be the subject of further research.

Acknowledgment

The authors would like to acknowledge the contribution of Hologram Industries (Dr. J. Sauvage-Vincent) in the experimental demonstration of the plasmon-triggered free-space wave switch in the wavelength domain.

References

[1] J. Sauvage-Vincent *et al.*, "Low-loss plasmon-triggered switching between reflected free-space diffraction orders," *Opt. Exp.*, vol. 22, no. 11, pp. 13 314–13 321, Jun. 2014.
[2] E. Popov, L. Tsonev, and D. Maystre, "Gratings—General properties of the Littrow mounting and energy flow distribution," *J. Modern Opt.*, vol. 37, no. 3, pp. 367–377, 1990.
[3] A. V. Tishchenko, "Numerical demonstration of the validity of the Rayleigh hypothesis," *Opt. Exp.*, vol. 17, no. 19, pp. 17 102–17 117, Sep. 2009.
[4] A. V. Tishchenko, O. Parriaux, and D. Neuschäfer, "Waveguide grating coupling of 2D focused beam under normal incidence: A phenomenological approach," in *Proc. SPIE*, 2004, vol. 5249, pp. 546–556.